The deglaciation of coastal areas of southeast Greenland

Laurence M. Dyke [a]*, Anna L. C. Hughes[b], Camilla S. Andresen[a], Anders A. Bjørk[c], Tavi Murray[d], John F. Hiemstra[d], Ángel Rodés[e]

[a] Geological Survey of Denmark and Greenland, Department of Glaciology and Climate, Øster Voldgade 10, DK-1350 Copenhagen K, Denmark.
[b] Department of Earth Science, University of Bergen and Bjerknes Centre for Climate Research, PO Box 7803, N-5020 Bergen, Norway.
[c] Centre for GeoGenetics, Natural History Museum of Denmark, University of Copenhagen, Øster Voldgade 5–7, DK-1350 Copenhagen K, Denmark.
[d] Glaciology Group, Swansea University, Singleton Park, Swansea, SA2 8PP, UK.
[e] NERC-CIAF, Scottish Universities Environmental Research Centre, East Kilbride, G75 0QF, UK.
* Corresponding author (laurencedyke@hotmail.com).

Abstract

Large marine-terminating glaciers around the margins of the Greenland Ice Sheet have retreated, accelerated, and thinned over the last two decades. Relatively little is known about the longer-term behaviour of the Greenland Ice Sheet, yet this information is valuable for assessing the significance of modern changes. We address this by reporting 11 new beryllium-10 (^{10}Be) exposure ages from previously uninvestigated coastal areas across southeast Greenland. The new ages are combined with existing data to assess the timing of glacier retreat across the region.

Results show that deglaciation occurred first in the north of the region (~68°N), and progressed southwards. This north-south progression is attributed to the influence of the warm Irminger Current on the ice margin. Areas in the south of the region were isolated from the warm waters by the shallow bathymetry of the continental shelf. This demonstrates that oceanographic forcing paced the deglaciation of southeast Greenland through the Younger Dryas and early Holocene. In most areas of southeast Greenland bedrock ages are systematically older than their counterpart boulder samples; this offset is likely the result of inherited ^{10}Be content in bedrock surfaces. This suggests that subglacial erosion during the last glacial cycle was insufficient to completely remove pre-existing ^{10}Be content. Alternatively, this pattern may be the signature of a substantial retreat and advance cycle prior to final Holocene deglaciation.

KEYWORDS: Quaternary; Glaciology; Greenland; Cosmogenic isotopes; ^{10}Be exposure dating; deglaciation.

1. Introduction

The southeast region of Greenland has experienced large glaciological changes in the last two decades. In the mid-2000s dynamic ice loss from the region dominated the mass budget of the wider Greenland Ice Sheet; this occurred as outlet glaciers across southeast Greenland synchronously retreated, accelerated, and thinned (Howat *et al.*, 2008; Murray *et al.*, 2010; Moon *et al.*, 2012; Enderlin *et al.*, 2014). Despite its obvious importance, relatively little is known about the glacial history of this region beyond the 20th century (Bjørk *et al.*, 2012; Khan *et al.*, 2014; Kjeldsen *et al.*, 2015). Reconstructing past glacier behaviour provides a baseline against which to assess the significance of modern changes.

Cosmogenic isotope dating has been used to reconstruct the glacial history in many areas around the periphery of Greenland (Sinclair *et al.*, 2016). In southeast Greenland investigations have focussed on the major fjord systems (Roberts *et al.*, 2008; Hughes *et al.*, 2012; Dyke *et al.*, 2014). Areas away from these high-discharge glaciers remain entirely

uninvestigated. Reconstructing the glacial history of these areas makes it possible to resolve differences in the timing, pattern, and style of deglaciation across the southeast region. This information is useful for assessing the performance of numerical models and for improving future predictions of ice sheet behaviour (e.g. Lecavalier *et al.*, 2014).

We present 11 new beryllium-10 (^{10}Be) exposure ages from four outer-coast locations in southeast Greenland (Figure 1). The data are presented together with photos, descriptions, and maps of the study areas to allow thorough interpretation of the ^{10}Be exposure ages from each site.

2. Study area: southeast Greenland

Southeast Greenland is a heavily glaciated, mountainous region containing many of the largest and fastest glaciers in Greenland. Cumulatively these marine-terminating glaciers drain 173,000 km^2 of the Greenland Ice Sheet (Rignot and Kanagaratnam, 2006).

The oceanography of southeast Greenland is dominated by southerly flowing boundary currents (Figure 1). Coastal surface waters (<300 m bsl) are characterised by cold, low-salinity currents that originate in the Arctic Ocean. These polar water masses flow southwards in the East Greenland Current and the East Greenland Coastal Current (Bacon *et al.*, 2002; Sutherland and Pickart, 2008). Warmer and more saline water, sourced from the subtropical Atlantic, is delivered to southeast Greenland by the Irminger Current (Straneo *et al.*, 2010; Brearley *et al.*, 2012). The Irminger Current circulates along the shelf-edge at depth (>300 m bsl) and invades the largest fjords through deep glacial troughs in the continental shelf (Straneo *et al.*, 2010; Sutherland *et al.*, 2013; Inall *et al.*, 2014).

The southeast region experiences a polar maritime climate. This is characterised by frequent low-pressure systems in autumn and winter months, and extended periods of high-pressure in the spring and summer (Hastings, 1960; Cappelen *et al.*, 2013). The mean (1961–1990) annual surface air temperature at Tasiilaq, in the centre of the region, is -1.7 °C (Cappelen *et al.*, 2001). Southeast Greenland experiences the highest precipitation rates in Greenland. Coastal areas in the centre of the sector receive more than 100 g cm^{-2} of precipitation annually (Bales *et al.*, 2009).

Unravelling the palaeoglaciological significance of each ^{10}Be sample requires a comprehensive understanding of each site. Geomorphological mapping of the study areas was undertaken using a combination of field observations, field photos, satellite imagery (Landsat 8), and high-resolution, orthorectified aerial photos (Korsgaard *et al.*, 2016). Four sites were investigated, and these are described individually in detail below.

2.1. Sampling site: Tugtilik

Tugtilik is a small fjord in the centre of the southeast region (Figure 1). The fjord is surrounded by mountainous terrain and the entrance is partially obstructed by Ailsa Ø (Similaq), a rocky island approximately 1.5 km long (Figure 3A). Small, land-terminating cirque glaciers (<2 km2) occupy favourable locations around the embayment (Figure 2A). A larger tidewater glacier (Tugtilip Kagtilersapia) lies 3 km to the northeast of the sampling site (Schjøtt, 2007b). The geomorphology of the area is relatively varied (Figure S1). High terrain is predominantly characterised by periglacial weathering features and shows little evidence of subglacial erosion (Figure 2A). At lower elevations (below around 800 m asl) the landscape is imprinted with landforms produced by mass-wasting, fluvial, lacustrine, and littoral processes (Figure S1).

Two erratic cobbles and an accompanying bedrock sample were collected from a prominent bedrock spur above a tributary of the main fjord (Figure 3A). Echo soundings and the

occurrence of numerous small grounded icebergs (Figure 2A) demonstrate that this embayment is shallow (<100 m deep, unpublished GLIMPSE Project data, 2011). Several small cirque glaciers are situated above the sampling site; these have single, unvegetated moraine complexes at their margins that are assumed to be of LIA age (e.g. Bjørk *et al.*, 2012; Bjørk *et al.*, 2018). Samples were collected from several hundred metres outboard of the closest moraine (Figure S1).

2.2. Sampling site: Ikertivaq

Ikertivaq is a heavily glaciated embayment in the centre of the southeast region (Figure 1). The bay is 40 km long, 20 km wide, and is the drainage portal for several large marine-terminating glaciers that drain 10,300 km^2 of the Greenland Ice Sheet (Rignot and Kanagaratnam, 2006). These glaciers flow at speeds in excess of 2 km a^{-1} and discharge around 23 Gt of ice annually (Rignot and Kanagaratnam, 2006; Enderlin *et al.*, 2014). Multibeam echo sounder data and gravimeter measurements show that a deep trough feature runs through the centre of Ikertivaq; this is more than 900 m below sea-level (bsl) in places (Fenty *et al.*, 2016; Millan *et al.*, 2018). The topography of the ice-free areas is subdued (<500 m asl, Schjøtt, 2007b) and has been heavily modified by glacial erosion. Depositional features are generally absent from Ikertivaq, except in a few land-terminating areas of the ice sheet. Here moraines are located within a few hundred metres of the present-day ice margin (Figure S2).

Samples for ^{10}Be dating were collected from an exposed bedrock ridge on Sûnikajik Island (Figures 2B and 3B). One erratic and one bedrock sample were collected from a glacially smoothed gneiss bedrock surface.

2.3. Sampling site: Køge Bugt

Køge Bugt is a large embayment in the centre of the southeast region (Figure 1). The bay is 40 km long and more than 20 km wide. The bathymetry of Køge Bugt has been partially mapped; multibeam echo sounder data demonstrates the presence of a central trough feature that is more than 700 m deep (Fenty *et al.*, 2016; Millan *et al.*, 2018). Køge Bugt is the drainage portal for several large marine-terminating outlet glaciers that drain approximately 30,000 km^2 of the Greenland Ice Sheet (Lewis and Smith, 2009, Figure 1). These glaciers flow at speeds of up to 5 km a^{-1} and discharge more than 40 Gt of ice annually (Rignot and Kanagaratnam, 2006; Enderlin *et al.*, 2014).

The ice-free areas are low-lying and characterised by erosional landforms; striated, streamlined gneiss bedrock dominates the landscape (Figure 2C). Field observations, Landsat 8 imagery, and aerial photographs (Korsgaard *et al.*, 2016) show that there are very few depositional features in the area. Minor moraines exist near the present-day ice margin (Figure S3). A small moraine also extends over the northern tip of Sipuliq Island (Figure 3C).

Rock samples for ^{10}Be dating were collected from Aqitseq Island (Figures 2C and 3C). A lack of suitable cobbles and boulders resulted in the collection of only one erratic rock sample. This was accompanied by a pair of bedrock samples that were obtained from a streamlined and striated gneiss surface nearby (Figure 2C).

2.4. Sampling site: Gerners Island

Gerners Island (Kulusuk) is part of a coastal archipelago approximately 30 km north of Gyldenløve Fjord (Figure 3D). Gerners Island covers an area of 17 km^2 and is 369 m asl at its highest point (Schjøtt, 2007a). The geomorphology of the island is characterised by glacially scoured gneiss bedrock, small perennial snow patches, numerous lakes and ponds, and limited sediment cover (Figures 2D and S4). Gerners Island lies several kilometres

offshore from Fridtjof Nansens Halvø, a mountainous, glaciated peninsula (Figure 3D). The peninsula hosts a small icefield (79.2 km^2) that is contiguous with the main body of the Greenland Ice Sheet (Rastner *et al.*, 2012). Kagtertôq, a 9 km wide channel, separates the sampling site from Jens Munks Island and Køge Bugt to the north (Figure 3D). Gyldenløve Fjord, to the south of Gerners Island, is a large fjord system and the drainage portal for several major tidewater glaciers (Figure 1).

Samples were collected from an exposed ridge on Gerners Island. Two erratic cobbles and a single bedrock sample were collected for ^{10}Be analysis from this site.

3. Sampling design and methods

3.1. ^{10}Be sampling design and procedure

Rock samples for ^{10}Be exposure dating were collected in 2011 from four outer-coast locations across central southeast Greenland (Figures 1–3). Samples were collected opportunistically during several research cruises along the coast. Samples were collected exclusively from low-elevation areas situated above the local marine limit. This was identified in the field by the occurrence of perched boulders (e.g. Long *et al.*, 2008). Samples were collected from bedrock that was free from vegetation and debris cover, and away from overshadowing terrain. Sampling sites were carefully located on prominent ridges; these are windswept and have experienced pronounced subglacial erosion. This approach mitigates shielding of rock samples by snow and minimises the potential for cosmogenic nuclide inheritance. Bedrock samples were collected from ice-scoured surfaces using a hammer and chisel (Figure 2C). Erratic samples consisted of whole, perched, rounded cobbles. Relatively heavy cobbles were chosen as these are unlikely to have been remobilised by the extreme katabatic winds that sporadically occur in the region (van As *et al.*, 2014). All samples were collected from quartz-rich lithologies that are suitable for ^{10}Be analysis.

Sample location and elevation were determined using a hand-held Garmin eTrex GPS unit with horizontal and vertical uncertainties of ~5 m and ~10 m respectively. Measurements of topographic shielding were taken at 30° intervals using a Suunto sighting clinometer. Additional measurements were undertaken, where necessary, to accurately characterise the horizon (Dunne *et al.*, 1999).

3.2. Sample preparation and ^{10}Be measurement

The surface of each rock sample was prepared for ^{10}Be analysis using standard mechanical and chemical procedures (Kohl and Nishiizumi, 1992; Child *et al.*, 2000; Wilson *et al.*, 2008). Samples were spiked with 200 mg of ^{9}Be carrier during quartz dissolution. The carrier used at the Cosmogenic Isotope Analysis Facility, where the samples were analysed, yields an average concentration of $2.7 \cdot 10^{-15} \pm 0.9 \cdot 10^{-15}$ ^{10}Be/^{9}Be. Measurements of ^{10}Be content were undertaken as part of a routine ^{10}Be run on the 5 Mv Pelletron tandem accelerator at the Scottish Universities Environmental Research Centre (Freeman *et al.*, 2007). Measured ^{10}Be/^{9}Be ratios were normalised to NIST SRM4325 material with an assumed ratio of $2.79 \cdot 10^{-11}$; this is equivalent to the 07KNSTD standard (Nishiizumi *et al.*, 2007).

3.3. ^{10}Be exposure age calculation

Exposure ages were calculated from ^{10}Be measurements using the online CRONUS-Earth calculator (version 2.2, http://hess.ess.washington.edu/math/). Exposure ages were calculated using the Arctic production rate (Young *et al.*, 2013) and Lal/Stone time-independent scaling (Lal, 1991; Stone, 2000). Exposure ages were calculated using individual correction factors for sample thickness, density, and topographic shielding (Table 1). No correction was applied to account for elevation changes caused by isostatic rebound.

This is assumed to be relatively minor as the majority of uplift occurred quickly during the Lateglacial and early Holocene (Bennike *et al.*, 2002; Long *et al.*, 2008). Exposure ages were calculated without applying a correction for erosion. Samples were collected exclusively from crystalline gneisses that are extremely resistant to weathering. The preservation of millimetre-scale glacial striations on gneiss surfaces up to ~11.8 ka BP old demonstrates that subaerial erosion rates in southeast Greenland are negligible over Holocene timescales (Dyke *et al.*, 2014).

Exposure ages are presented in thousands of years before sample collection (ka BP) and are accompanied by internal uncertainties. The standard deviation is given as the measure of uncertainty where the mean of several samples has been calculated (Dunai, 2010).

4. Results

We present 11 new ^{10}Be exposure ages from coastal locations across southeast Greenland (Figures 3–4). Sample details and accelerator mass spectrometry results are presented in Table 1.

4.1. Tugtilik

Two erratic cobbles from Tugtilik are dated to 11.0 ±0.4 and 9.3 ±0.4 ka BP, the accompanying bedrock sample has an exposure age of 9.8 ±0.4 ka BP (Figure 3A). The sample site is characterised by a low-discharge glaciological regime and is surrounded by small, land-terminating cirque glaciers (Section 3.1). Geomorphological mapping (Figure S1) and field observations indicate that glacial erosion has been limited in this setting. It is plausible that both bedrock and erratic samples contain inherited ^{10}Be as slow-moving, polythermal cirque glaciers are inefficient at both eroding bedrock and removing pre-existing subglacial erratics from their catchments. In comparable settings in central East Greenland the youngest boulder samples have been used to determine the timing of deglaciation (Hall *et al.*, 2008a; Hall *et al.*, 2008b; Kelly *et al.*, 2008). This approach is adopted for the samples from Tugtilik. The older erratic and bedrock ^{10}Be ages probably reflect substantial quantities of inherited ^{10}Be. The youngest erratic ^{10}Be age best represents the final deglaciation of Tugtilik, which occurred at 9.3 ±0.4 ka BP.

4.2. Ikertivaq

The erratic cobble from Sûnikajik Island is dated to 9.9 ±0.4 ka BP, the accompanying bedrock sample yields an exposure age of 11.4 ±0.7 ka BP (Figure 3B). Ikertivaq is characterised by glacially scoured, streamlined bedrock (Figure S2). This suggests that the area was completely overrun by fast-flowing ice during the last glaciation. Intense ice streaming would have removed all pre-existing erratics from the landscape. Consequently, boulder samples from this area are unlikely to contain inherited ^{10}Be and we use the erratic exposure age (9.9 ±0.4 ka BP) to constrain the timing of deglaciation in this area. The bedrock sample is almost 2 ka older and probably contains inherited ^{10}Be. We consider this sample to be anomalously old.

4.3. Køge Bugt

The single erratic sample from Aqitseq Island, in Køge Bugt, yields an exposure age of 11.2 ±0.4 ka BP. The accompanying bedrock samples have exposure ages of 9.2 ±0.4 and 10.5 ±0.4 ka BP (Figure 3C). The erratic sample is substantially older than its bedrock counterparts; this is uncommon in high-discharge glacial systems (Hughes *et al.*, 2012; Dyke *et al.*, 2014). There are several explanations that may account for this. The erratic could be anomalously old as a result of inherited ^{10}Be content. We consider this implausible as Køge Bugt experienced intense glacial erosion during the last glaciation (Figure S3) and it is very

unlikely that pre-existing erratics remained on the landscape through glacial inundation. Alternatively, the bedrock samples may have been shielded by sediment or snow cover after deglaciation; this would result in anomalously young ages. However, there is no geomorphological evidence that the sample site has been covered by sediment during the Holocene. Snow cover is also considered unlikely. The samples were collected from an exposed, windswept ridge where snow cover is intrinsically limited. Furthermore, all samples were taken from the same surface and sediment or snow cover would affect all samples similarly. The difference between erratic and bedrock ^{10}Be exposure ages remains unexplained.

Cosmogenic isotope dates from Køge Bugt are complimented by recently reported ^{14}C dates from a marine sediment core obtained from the centre of the bay (Figures 1 and 3C, Dyke *et al.*, 2017). Results from the core demonstrate that Køge Bugt has been characterised by open glaciomarine conditions from at least 9.1 ±0.2 thousand calibrated years before present (cal. ka BP). The basal ^{14}C date provides an absolute minimum constraint on the timing of deglaciation here and we infer that this area of Køge Bugt had deglaciated substantially before this time. The overlap between the ^{14}C date (9.1 ±0.2 cal. ka BP) and the youngest ^{10}Be exposure age (9.2 ±0.4 ka BP) suggests that this ^{10}Be age is anomalously young. Additionally, the exposure age of this sample does not overlap within errors with either of the other samples from this site. Consequently, we exclude the youngest bedrock ^{10}Be age from further analysis. For consistency with other sites across southeast Greenland we use the erratic exposure age (11.2 ±0.4 ka BP) to track the timing of deglaciation in Køge Bugt. However, it is important to note that we use this age tentatively.

4.4. Gerners Island

Erratic samples from Gerners Island, to the north of Gyldenløve Fjord, yield exposure ages of 9.8 ±0.5 and 10.1 ±0.4 ka BP. These ages are concordant and overlap within uncertainties (Figure 3D). The accompanying bedrock sample is significantly older (11.4 ±0.7 ka BP) and does not overlap within error with the erratic exposure ages from this locality. The bedrock sample likely contains inherited ^{10}Be. The erratic samples are considered to accurately constrain the timing of deglaciation at this site. The mean and standard deviation of the erratic samples (9.9 ±0.2 ka BP) are used for further analysis and discussion. The sampling site is located between Gyldenløve Fjord and Kagtertôq (Figure 3D). These large channel features would have hosted substantial ice streams during the LGM and the timing of deglaciation at Gerners Island probably reflects the retreat and separation of these glacier systems.

5. Discussion

5.1. Using ^{10}Be dates to determine the timing of deglaciation

We present new ^{10}Be exposure ages from outer-coast areas of southeast Greenland. The results indicate that deglaciation occurred in these areas between 11.2 and 9.3 ka BP (Figures 3–4). The geomorphology of Ikertivaq, Køge Bugt, and Gerners Island is characterised by features formed through intense glacial erosion (Figures S1–S4). A wide range of geomorphological features at macro-, meso-, and micro-scales suggest that these areas experienced intense glacial erosion beneath high-discharge ice streams during the last glaciation. Erratic samples from high-discharge settings generally provide a reliable record of the timing of deglaciation (e.g. Roberts *et al.*, 2009; Hughes *et al.*, 2012; Winsor *et al.*, 2015). Consequently, we use the mean ^{10}Be exposure age of erratics to determine the timing of deglaciation at each of these sites.

The sampling site at Tugtilik is fundamentally different to the areas further south. The site is sheltered from the main body of the Greenland Ice Sheet by high coastal mountains and is

located away from major outlet glaciers (Figure 3A). Geomorphological mapping further highlights the differences between Tugtilik and the other sampling sites (Figures S1–4). The sampling sites at Ikertivaq, Køge Bugt, and Gerners Island are all characterised by glacially-scoured bedrock and the absence of depositional features (Figure 2). In contrast, Tugtilik has varied geomorphology that includes both depositional and periglacial features (Figure S1). We interpret this as evidence that Tugtilik experienced a low-discharge regime during glacial inundation (Glasser and Bennet, 2004). Consequently, we treat the ^{10}Be exposure ages from Tugtilik differently, the youngest erratic age from this site is used to determine the timing of deglaciation (e.g. Hall *et al.*, 2008b; Kelly *et al.*, 2008).

5.2. The timing of deglaciation in southeast Greenland

New ^{10}Be dates from outer-coast areas of southeast Greenland complement existing data from the large fjords in the region (Hughes *et al.*, 2012; Dyke *et al.*, 2014). When compiled, the ^{10}Be data indicate that the deglaciation of the coast occurred first in the north of the sector, and progressed southwards during the early Holocene (Figure 4). Adjacent glacier systems in southeast Greenland deglaciated in broad synchronicity (i.e. within error). However, there is a more substantial difference in the timing of deglaciation between Kangerdlugssuaq Fjord (11.8 ±0.7 ka BP), in the north of the sector, and Bernstorffs Fjord (10.4 ±0.7 ka BP) and Gerners Island (9.9 ±0.2 ka BP), in the south of the region (Figure 4). It is important to note that this trend is not particularly robust (R2 = 0.46), but there is an obvious pattern of deglaciation occurring first in the north, before progressing southwards.

We promulgate the hypothesis of Dyke *et al.* (2014) and suggest that the deglaciation of the coast in southeast Greenland was initially driven by the incursion of warm water from the Irminger Current. However, the impact of the Irminger Current on individual glacier systems was moderated by the local coastal bathymetry. Incursion of warm Atlantic water into Kangerdlugssuaq Trough triggered the deglaciation of Kangerdlugssuaq Fjord at around 11.8 ka BP (Figure 4). This occurred during cold climatic conditions at the end of the Younger Dryas stadial (Jennings *et al.*, 2006; Dyke *et al.*, 2014). Kangerdlugssuaq Glacier is particularly susceptible to oceanographic forcing as it is closest to the source of warm Atlantic Water and the deep, straight canyon of Kangerdlugssuaq Trough allows the Irminger Current to easily penetrate the continental shelf (Figures 1 and 4). The large glacier systems further south deglaciated later, between approximately 11.2 and 9.9 ka BP (Figure 4). These systems have sinuous troughs and areas of shallow bathymetry offshore, and this limited the incursion of the Irminger Current to these glaciers during the Younger Dryas (Figure 4, Sutherland *et al.*, 2013; Fenty *et al.*, 2016). The retreat of glaciers in the centre of southeast Greenland occurred during the early Holocene and appears to have been driven primarily by the pronounced climatic warming during this interval (Hughes *et al.*, 2012; Dyke *et al.*, 2014).

The latitudinal trend in the timing of deglaciation may have been accentuated by freshening and cooling of the warm Irminger Current by meltwater and icebergs produced during the deglaciation of Kangerdlugssuaq Fjord. This would have reduced its capacity to melt marine-terminating glaciers downstream. Modern oceanographic measurements provide an analogue for this hypothesis. The freshwater content in surface currents off southeast Greenland increases by 60% from 68 to 60°N due to the combined input of glacier runoff, iceberg melt, and sea-ice melt (Sutherland and Pickart, 2008). Glacier retreat and ice discharge during the late Younger Dryas and early Holocene was at least as fast as the present-day (Hughes *et al.*, 2012; Dyke *et al.*, 2014), and it is likely that this effect was more pronounced during the large scale deglaciation occurring in this interval.

5.3. Inheritance of ^{10}Be in bedrock samples

Bedrock samples from Ikertivaq and Gerners Island are substantially older than their erratic counterparts. We note that this pattern is not universal in the data presented here, bedrock

samples from Køge Bugt are younger than the accompanying erratic and the bedrock exposure age from Tugtilik is bracketed by the erratic exposure ages (Figure 4). However, the offset between erratic and bedrock ages is clearer when the data from across the region are compiled (Hughes *et al.*, 2012; Dyke *et al.*, 2014). The compiled data show a reasonably consistent and systematic offset, of around 1 ka, between erratic and boulder exposure ages (Figure 4).

The excess ^{10}Be content in bedrock surfaces across much of the region suggests that glacial erosion was not sufficient to completely remove ^{10}Be from previous periods of exposure. The origin of the inherited ^{10}Be in bedrock samples is unclear. It may simply reflect erosion of less than 3 m through the last glacial cycle (Gosse and Phillips, 2001). Alternatively, the pattern of young erratics on bedrock with minor ^{10}Be inheritance could be the signature of a short-lived glacial readvance event that occurred after initial deglaciation. This 'scrubbed' existing erratics from the landscape, but was insufficient to remove ^{10}Be that accumulated during the ice-free conditions before the subsequent readvance. We speculate that this readvance may have occurred during the YD. The evidence for this scenario is, at best, circumstantial. However, it is possible to test with additional targeted investigation. High resolution numerical glacier modelling and ^{10}Be exposure ages from vertical `dipstick' transects within the major fjord systems offer an opportunity to resolve this hypothesis. Further investigation is required.

6. Conclusions

The compilation of new and existing ^{10}Be age determinations from coastal locations across southeast Greenland confirm that deglaciation occurred first in the north of the sector and progressed southwards. This pattern of deglaciation is attributed to the varying influence of the Irminger Current on the ice margin that, in turn, was moderated by the bathymetry of the continental shelf. This demonstrates that oceanographic forcing was important in pacing glacier retreat in southeast Greenland through the Younger Dryas and early Holocene along the entire length of the coast.

In most areas of southeast Greenland bedrock ages are systematically older than their counterpart boulder samples. The offset reflects the presence of excess ^{10}Be in bedrock surfaces, inherited from previous periods of exposure. This may indicate that subglacial erosion during the last glacial cycle was insufficient to completely remove pre-existing ^{10}Be content. Alternatively, this pattern may be the signature of a substantial glacial retreat and advance cycle prior to final Holocene deglaciation.

7. Acknowledgements

This manuscript is a contribution to the "Past and future dynamics of the Greenland Ice Sheet: what is the ocean hiding?" Project (Camilla Andresen; VILLUM Foundation, 10100). This project was conceived and samples were collected whilst Laurence Dyke was in receipt of a NERC CASE doctoral scholarship (NE/I528126/1). Samples were processed and analysed with support from a NERC CIAF grant (Laurence Dyke; 9123.0412). Fieldwork was supported by the Leverhulme Trust (Tavi Murray; GLIMPSE Project, F/00391/J) and National Geographic (Tavi Murray; 111741). Additional fieldwork was funded by the Danish Independent Research Council (FNU), the Danish Centre for Sea Research (DCH), and Geocenter Denmark (Camilla Andresen; SEDIMICE Project). We thank the captain (Sigurður Petturson) and crew of M/V Þytur for their assistance during fieldwork.

References

Bacon, S., Reverdin, G., Rigor, I. G., Snaith, H. M., 2002. A freshwater jet on the east Greenland shelf. *Journal of Geophysical Research: Oceans* **107**: 1–18.

Balco, G., 2011. Contributions and unrealized potential contributions of cosmogenic-nuclide exposure dating to glacier chronology, 1990–2010. *Quaternary Science Reviews* **30**: 3–27.

Balco, G., Briner, J. P., Finkel, R. C., Rayburn, J. A., Ridge, J. C., Schaefer, J. M., 2009. Regional beryllium-10 production rate calibration for late-glacial northeastern North America. *Quaternary Geochronology* **4**: 93–107.

Bales, R. C., Guo, Q., Shen, D., McConnell, J. R., Du, G., Burkhart, J. F., Spikes, V. B., Hanna, E., Cappelen, J., 2009. Annual accumulation for Greenland updated using ice core data developed during 2000–2006 and analysis of daily coastal meteorological data. *Journal of Geophysical Research: Atmospheres* **114**: 1–14.

Bennike, O., Björck, S., Lambeck, K., 2002. Estimates of South Greenland late-glacial ice limits from a new relative sea level curve. *Earth and Planetary Science Letters* **197**: 171–186.

Bjørk, A. A., Kjær, K. H., Korsgaard, N. J., Khan, S. A., Kjeldsen, K. K., Andresen, C. S., Box, J. E., Larsen, N. K., Funder, S., 2012. An aerial view of 80 years of climate-related glacier fluctuations in southeast Greenland. *Nature Geoscience* **5**: 427–432.

Bjørk, A. A. and Aagaard, S. and Lütt, A. and Khan, S. A. and Box, J. E. and Kjeldsen, K. K. and Larsen, N. K. and Korsgaard, N. J. and Cappelen, J. and Colgan, W. T. and Machguth, H. and Andresen, C. S. and Peings, Y. and Kjær, K. H., 2017. Changes in Greenland's peripheral glaciers linked to the North Atlantic Oscillation. *Nature Climate Change* **8**(1): 48–52.

Brearley, J. A., Pickart, R. S., Valdimarsson, H., Jonsson, S., Schmitt, R. S. W., Haine, T. W. N., 2012. The East Greenland boundary current system south of Denmark Strait. *Deep-Sea Research Part I: Oceanographic Research Papers* **63**: 1–19.

Cappelen, J., Jørgensen, B. V., Laursen, E. V., Stannius, L. S., Thomsen, R. S., 2001. *The Observed Climate of Greenland, 1958–99 — with Climatological Standard Normals*, 1961–1990. Tech. Rep. 00-18, Danish Meteorological Institution, 152 pp.

Cappelen, J., Kern-Hansen, C., Laursen, E. V., Jørgensen, P. V., 2013. *Greenland - DMI Historical Climate Data Collection 1873–2012*. Tech. Rep. 13-04, Danish Meteorological Institution, 75 pp.

Child, D., Elliott, G., Mifsud, C., Smith, A. M., Fink, D., 2000. Sample processing for earth science studies at ANTARES. *Nuclear Instruments and Methods in Physics Research Section B: Beam Interactions with Materials and Atoms* **172**: 856–860.

Dunai, T. J., 2010. *Cosmogenic Nuclides*. Cambridge University Press, Cambridge, UK, 198 pp.

Dunne, J., Elmore, D., Muzikar, P., 1999. Scaling factors for the rates of production of cosmogenic nuclides for geometric shielding and attenuation at depth on sloped surfaces. *Geomorphology* **27**: 3–11.

Dyke, L. M., Hughes, A. L. C., Murray, T., Hiemstra, J. F., Andresen, C. S., Rodés, Á., 2014. Evidence for the asynchronous retreat of large outlet glaciers in southeast Greenland at the end of the last glaciation. *Quaternary Science Reviews* **99**: 244–259.

Dyke, L. M., Andresen, C. S., Seidenkrantz, M.-S., Hughes, A. L. C., Hiemstra, J. F., Murray, T., Bjørk, A. A., Sutherland, D. A., Vermassen, F., 2017. Minimal Holocene retreat of large tidewater glaciers in Køge Bugt, southeast Greenland. *Scientific Reports* **7**(12330): 1–10.

Enderlin, E. M., Howat, I. M., Jeong, S., Noh, M.-J., van Angelen, J. H., van den Broeke, M. R., 2014. An improved mass budget for the Greenland ice sheet. *Geophysical Research Letters* **41**: 866–872.

Fenty, I., Willis, J. K., Khazendar, A., Dinardo, S., Forsberg, R., Fukumori, I., Holland, D., Jakobsson, M., Moller, D., Morison, J., Münchow, A., Rignot, E., Schodlok, M., Thompson, A. F., Tinto, K.,

Rutherford, M. and Trenholm, N., 2016. Oceans Melting Greenland: Early results from NASA's ocean-ice mission in Greenland. *Oceanography* **29**(4): 72–83.

Freeman, S., Bishop, P., Bryant, C., Cook, G., Dougans, D., Ertunc, T., Fallick, A., Ganeshram, R., Maden, C., Naysmith, P., Schnabel, C., Scott, M., Summerfield, M., Xu, S., 2007. The SUERC AMS laboratory after 3 years. *Nuclear Instruments and Methods in Physics Research Section B: Beam Interactions with Materials and Atoms* **259**: 66–70.

Glasser, N. F., Bennett, M. R., 2004. Glacial erosional landforms: origins and significance for palaeoglaciology. *Progress in Physical Geography* **28**: 43–75.

Gosse, J. C., Phillips, F. M., 2001. Terrestrial in situ cosmogenic nuclides: theory and application. *Quaternary Science Reviews* **20**: 1475–1560.

Hall, B., Baroni, C., Denton, G., Kelly, M. A., Lowell, T., 2008a. Relative sea-level change, Kjove Land, Scoresby Sund, East Greenland: Implications for seasonality in Younger Dryas time. *Quaternary Science Reviews* **27**: 2283–2291.

Hall, B. L., Baroni, C., Denton, G. H., 2008b. The most extensive Holocene advance in the Stauning Alper, East Greenland, occurred in the Little Ice Age. *Polar Research* **27**: 128–134.

Hastings, Jr., A. D., 1960. *Environment of southeast Greenland*. Tech. Rep. EP-140, Quartermaster Research and Engineering Center, Environmental Protection Research Division, Natick, Massachusetts, 79 pp.

Howat, I. M., Joughin, I., Fahnestock, M., Smith, B. E., Scambos, T. A., 2008. Synchronous retreat and acceleration of southeast Greenland outlet glaciers 2000–06: ice dynamics and coupling to climate. *Journal of Glaciology* **54**: 646–660.

Howat, I. M., Negrete, A., Smith, B. E., 2014. The Greenland Ice Mapping Project (GIMP) land classification and surface elevation datasets. *The Cryosphere* **8**: 1509–1518.

Hughes, A. L. C., Rainsley, E., Murray, T., Fogwill, C. J., Schnabel, C., Xu, S., 2012. Rapid response of Helheim Glacier, southeast Greenland, to early Holocene climate warming. *Geology* **40**: 427–430.

Inall, M. E., Murray, T., Cottier, F. R., Scharrer, K., Boyd, T. J., Heywood, K. J., Bevan, S. L., 2014. Oceanic heat delivery via Kangerdlugssuaq Fjord to the south-east Greenland ice sheet. *Journal of Geophysical Research: Oceans* **119**: 631–645.

Jakobsson, M., Mayer, L., Coakley, B., Dowdeswell, J. A., Forbes, S., Fridman, B., Hodnesdal, H., Noormets, R., Pedersen, R., Rebesco, M., Schenke, H. W., Zarayskaya, Y., Accettella, D., Armstrong, A., Anderson, R. M., Bienhoff, P., Camerlenghi, A., Church, I., Edwards, M., Gardner, J. V., Hall, J. K., Hell, B., Hestvik, O., Kristoffersen, Y., Marcussen, C., Mohammad, R., Mosher, D., Nghiem, S. V., Pedrosa, M. T., Travaglini, P. G., Weatherall, P., 2012. The International Bathymetric Chart of the Arctic Ocean (IBCAO) Version 3.0. *Geophysical Research Letters* **39**: L12609

Jennings, A. E., Hald, M., Smith, M., Andrews, J. T., 2006. Freshwater forcing from the Greenland Ice Sheet during the Younger Dryas: evidence from southeastern Greenland shelf cores. *Quaternary Science Reviews* **25**: 282–298.

Kelly, M. A., Lowell, T. V., Hall, B. L., Schaefer, J. M., Finkel, R. C., Goehring, B. M., Alley, R. B., Denton, G. H., 2008. A ^{10}Be chronology of lateglacial and Holocene mountain glaciation in the Scoresby Sund region, east Greenland: implications for seasonality during lateglacial time. *Quaternary Science Reviews* **27**: 2273–2282.

Khan, S. A., Kjeldsen, K. K., Kjær, K. H., Bevan, S., Luckman, A., Aschwanden, A., Korsgaard, N. J., Bjørk, A. A., Box, J. E., van den Broeke, M., van Dam, T. M., Fitzner, A., 2014. Glacier dynamics at Helheim and Kangerdlugssuaq glaciers, southeast Greenland, since the Little Ice Age. *The Cryosphere* **8**: 1497–1507.

Kjeldsen, K. K., Korsgaard, N. J., Bjørk, A. A., Khan, S. A., Box, J. E., Funder, S., Larsen, N. K., Bamber, J. L., Colgan, W., van den Broeke, M., Siggaard-Andersen, M.-L., Nuth, C., Schomacker, A., Andresen, C. S., Willerslev, E., Kjær, K. H., 2015. Spatial and temporal distribution of mass loss from the Greenland Ice Sheet since AD 1900. *Nature* **528**: 396–400.

Kohl, C. P., Nishiizumi, K., 1992. Chemical isolation of quartz for measurement of in-situ-produced cosmogenic nuclides. *Geochimica et Cosmochimica Acta* **56**: 3583–3587.

Korsgaard, N. J., Nuth, C., Khan, S. A., Kjeldsen, K. K., Bjørk, A. A., Schomacker, A., Kjær, K. H., 2016. Digital elevation model and orthophotographs of Greenland based on aerial photographs from 1978–1987. *Scientific Data* **3**: 1–15.

Lal, D., 1991. Cosmic ray labeling of erosion surfaces: in situ nuclide production rates and erosion models. *Earth and Planetary Science Letters* **104**: 424–439.

Lecavalier, B. S., Milne, G. A., Simpson, M. J. R., Wake, L., Huybrechts, P., Tarasov, L., Kjeldsen, K. K., Funder, S., Long, A. J., Woodroffe, S., Dyke, A. S., Larsen, N. K., 2014. A model of Greenland ice sheet deglaciation constrained by observations of relative sea level and ice extent. *Quaternary Science Reviews* **102**: 54–84.

Lewis, S. M., Smith, L. C., 2009. Hydrologic drainage of the Greenland Ice Sheet. *Hydrological Processes* **23**: 2004–2011.

Long, A. J., Roberts, D. H., Simpson, M. J. R., Dawson, S., Milne, G. A., Huybrechts, P., 2008. Late Weichselian relative sea-level changes and ice sheet history in southeast Greenland. *Earth and Planetary Science Letters* **272**: 8–18.

Millan, R. and Rignot, E. and Mouginot, J. and Wood, M. and Bjørk, A. A. and Morlighem, M., 2018. Vulnerability of Southeast Greenland glaciers to warm Atlantic Water from Operation IceBridge and Ocean Melting Greenland data. *Geophysical Research Letters* DOI: 10.1002/2017GL076561.

Moon, T., Joughin, I., Smith, B., Howat, I., 2012. 21st-Century Evolution of Greenland Outlet Glacier Velocities. *Science* **336**: 576–578.

Murray, T., Scharrer, K., James, T. D., Dye, S. R., Hanna, E., Booth, A. D., Selmes, N., Luckman, A., Hughes, A. L. C., Cook, S., Huybrechts, P., 2010. Ocean regulation hypothesis for glacier dynamics in southeast Greenland and implications for ice sheet mass changes. *Journal of Geophysical Research: Earth Surface* **115**: F03026.

Nishiizumi, K., Imamura, M., Caffee, M. W., Southon, J. R., Finkel, R. C., McAninch, J., 2007. Absolute calibration of ^{10}Be AMS standards. *Nuclear Instruments and Methods in Physics Research Section B: Beam Interactions with Materials and Atoms* **258**: 403–413.

Ó Cofaigh, C. A., Dowdeswell, J. A., 2001. Laminated sediments in glacimarine environments: diagnostic criteria for their interpretation. *Quaternary Science Reviews* **20**: 1411–1436.

Rastner, P., Bolch, T., Mölg, N., Machguth, H., Le Bris, R., Paul, F., 2012. The first complete inventory of the local glaciers and ice caps on Greenland. *The Cryosphere* **6**: 1483–1495.

Rignot, E., Kanagaratnam, P., 2006. Changes in the Velocity Structure of the Greenland Ice Sheet. *Science* **311**: 986–990.

Roberts, D. H., Long, A. J., Schnabel, C., Davies, B. J., Xu, S., Simpson, M. J. R., Huybrechts, P., 2009. Ice sheet extent and early deglacial history of the southwestern sector of the Greenland Ice Sheet. *Quaternary Science Reviews* **28**: 2760–2773.

Roberts, D. H., Long, A. J., Schnabel, C., Freeman, S., Simpson, M. J. R., 2008. The deglacial history of southeast sector of The Greenland Ice Sheet during the Last Glacial Maximum. *Quaternary Science Reviews* **27**: 1505–1516.

Schjøtt, T., 2007a. Saqqisikuik: Skjoldungen, 1:500,000. *Saga Maps Viking Polar Cruise Series*, 1.

Schjøtt, T., 2007b. Tasiilaq: Angmagssalik, 1:500,000. *Saga Maps Viking Polar Cruise Series*, 1.

Sinclair, G., Carlson, A. E., Mix, A. C., Lecavalier, B. S., Milne, G., Mathias, A., Buizert, C., DeConto, R., 2016. Diachronous retreat of the Greenland ice sheet during the last deglaciation. *Quaternary Science Reviews* **145**: 243–258.

Stone, J. O., 2000. Air pressure and cosmogenic isotope production. *Journal of Geophysical Research* **105**: 23,753–23,760.

Straneo, F., Hamilton, G. S., Sutherland, D. A., Stearns, L. A., Davidson, F., Hammill, M. O., Stenson, G. B., Rosing-Asvid, A., 2010. Rapid circulation of warm subtropical waters in a major glacial fjord in East Greenland. *Nature Geoscience* **3**: 182–186.

Sutherland, D. A., Pickart, R. S., 2008. The East Greenland Coastal Current: Structure, variability, and forcing. Progress In Oceanography **78**: 58–77.

Sutherland, D. A., Straneo, F., Stenson, G. B., Davidson, F. J. M., Hammill, M. O., Rosing-Asvid, A., 2013. Atlantic water variability on the SE Greenland continental shelf and its relationship to SST and bathymetry. *Journal of Geophysical Research: Oceans* **118**: 1–9.

van As, D., Fausto, R. S., Steffen, K., Ahlstrøm, A. P., Andersen, S. B., Andersen, M. L., Box, J. E., Charalampidis, C., Citterio, M., Colgan, W. T., Edelvang, K., Larsen, S. H., Nielsen, S., Veicherts, M., Weidick, A., 2014. Katabatic winds and piteraq storms: observations from the Greenland ice sheet. *Geological Survey of Denmark and Greenland Bulletin* **31**: 83–86.

Wilson, P., Bentley, M. J., Schnabel, C., Clark, R., Xu, S., 2008. Stone run (block stream) formation in the Falkland Islands over several cold stages, deduced from cosmogenic isotope (^{10}Be and ^{26}Al) surface exposure dating. *Journal of Quaternary Science* **23**: 461–473.

Winsor, K., Carlson, A. E., Caffee, M. W., Rood, D. H., 2015. Rapid last-deglacial thinning and retreat of the marine-terminating southwestern Greenland ice sheet. *Earth and Planetary Science Letters* **426**: 1–12.

Young, N., Schaefer, J. M., Briner, J. P., Goehring, B. M., 2013. A ^{10}Be production-rate calibration for the Arctic. *Journal of Quaternary Science* **28**: 515–526.

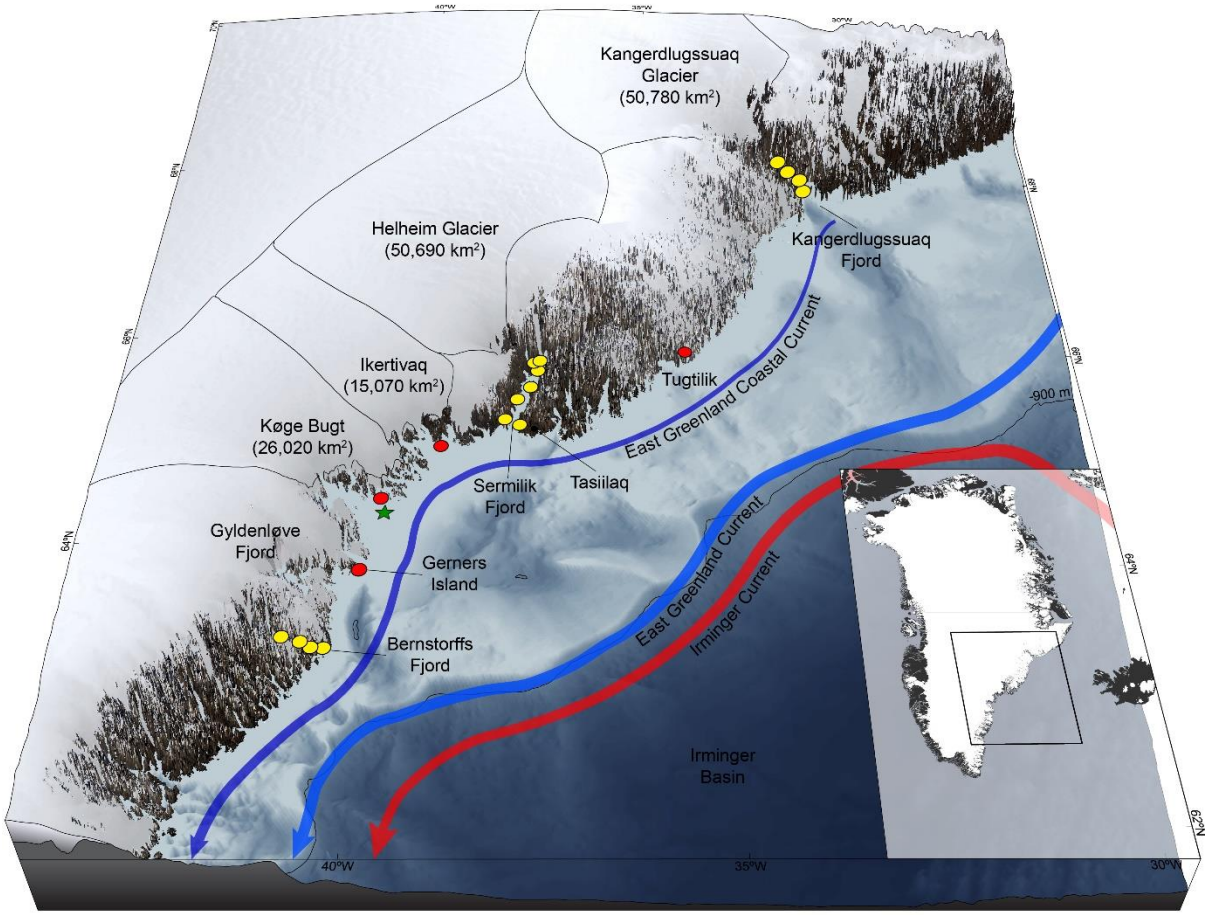

Figure 1: Map of southeast Greenland showing the location of sites in this study (20x vertical exaggeration). The inset map shows the extent of the main figure. Red circles denote ^{10}Be sampling sites in this study, the green star marks the location of sediment core ER1116 (Dyke *et al.*, 2017). The location of previously published ^{10}Be and ^{26}Al exposure ages are shown by the yellow circles. Bathymetric data are from Jakobsson *et al.* (2012). Surface ocean currents are adapted from Sutherland and Pickart (2008). Individual present-day drainage basins are shown for Kangerdlugssuaq and Helheim Glaciers. Composite basins are shown for the glaciers draining into Ikertivaq and Køge Bugt. Individual drainage basins are not available for Gyldenløve Fjord or Bernstorffs Fjord. Terrestrial imagery is a composite mosaic of Landsat 8 scenes draped onto elevation data from Howat *et al.* (2014).

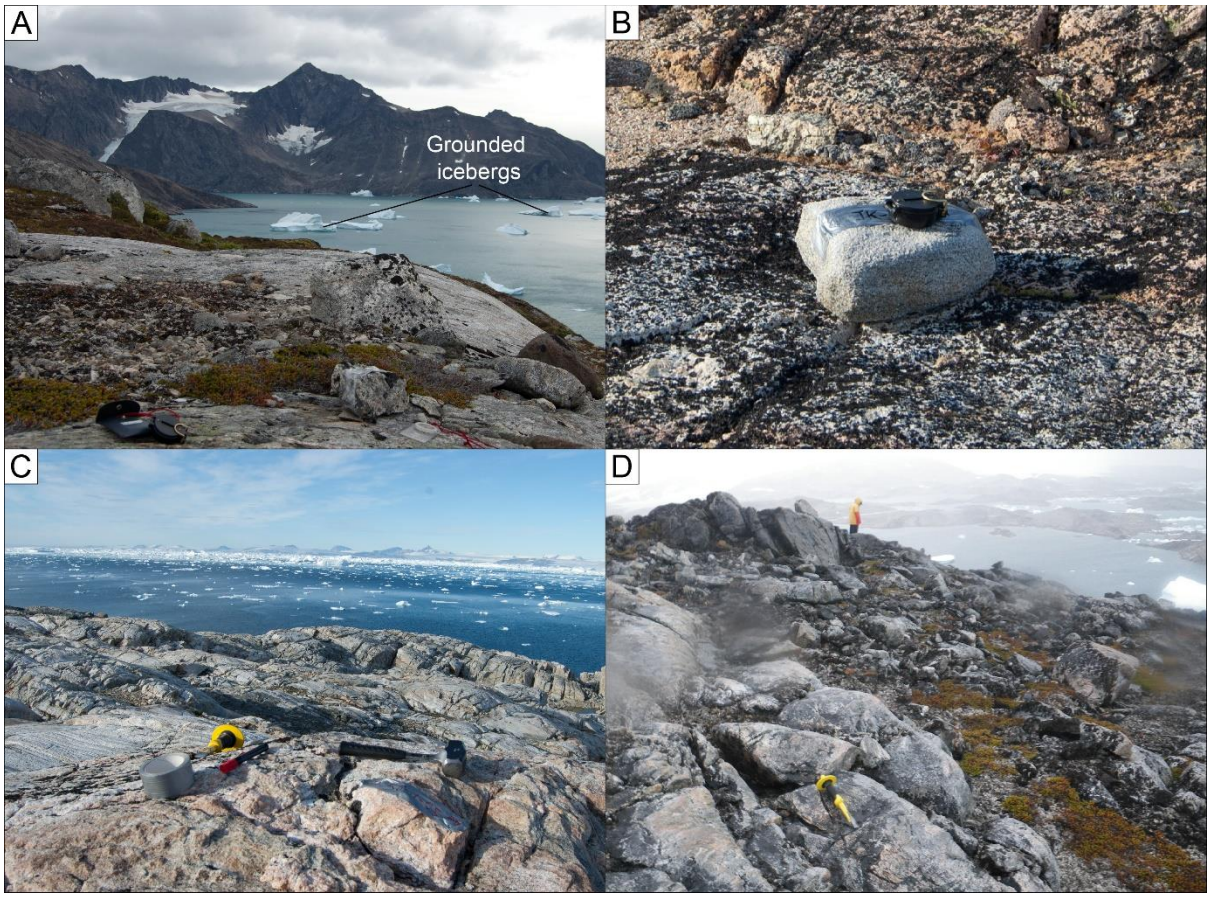

Figure 2: Field area photos. A: Sampling site at Tugtilik. B: Erratic sample from Sûnikajik, a small island in Ikertivaq. Compass for scale is 10 cm across. C: Aqitseq, Køge Bugt. Bedrock sampling site in foreground (lump hammer for scale, ~30 cm long). D: Gerners Island (Kulusuk), near Gyldenløve Fjord. Sampled bedrock in foreground (the chisel, for scale, is 31 cm long). Focal aberrations are caused by water on the camera lens; samples were collected during storm conditions. The location and approximate field-of-view (where appropriate) of each photo is shown in Figure 3.

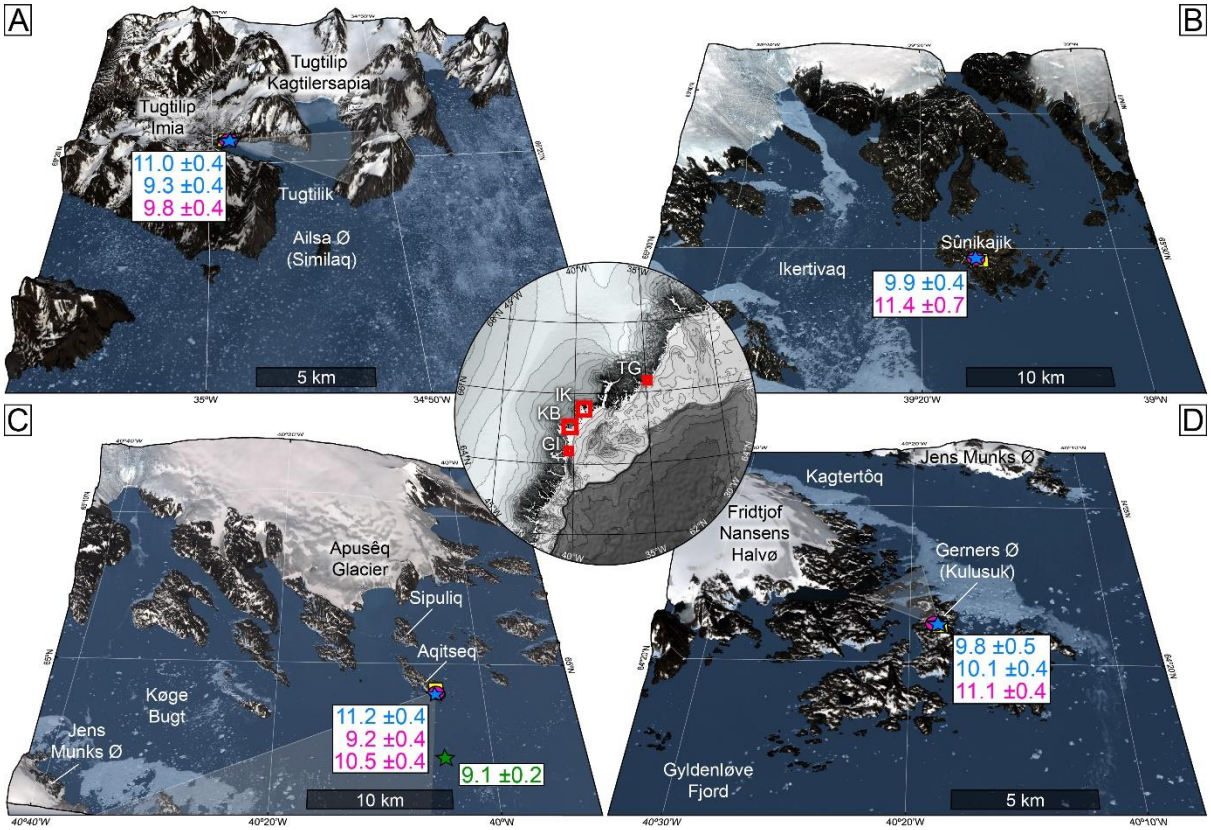

Figure 3: Bedrock and erratic ^{10}Be exposure ages from southeast Greenland. A: Tugtilik (TG), 2x vertical exaggeration. B: Ikertivaq (IK), 4x vertical exaggeration. C: Køge Bugt (KB), 4x vertical exaggeration. D: Gerners Island (GI), 2x vertical exaggeration. Background imagery are Landsat 8 scenes draped on elevation data from Howat *et al.* (2014). The inset map shows the location and extent of maps A–D (red boxes). Erratic samples are shown in blue. Bedrock samples are shown in magenta. Yellow squares show the location of photos in Figure 2; the field-of-view is shown by the grey shading.

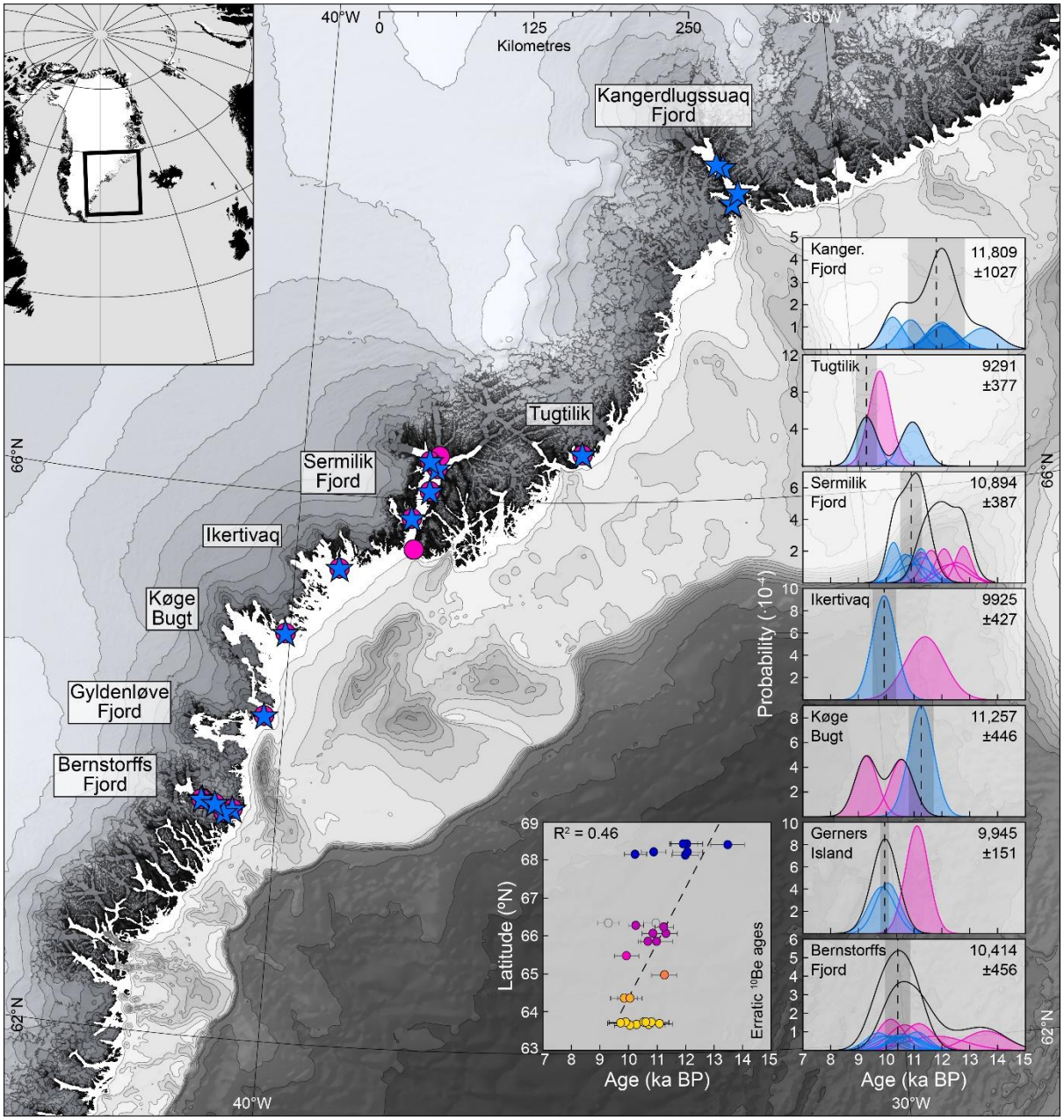

Figure 4. Map of ^{10}Be exposure dates from southeast Greenland (Hughes *et al.*, 2012; Dyke *et al.*, 2014, and this study). Terrestrial elevation data are from Howat *et al.* (2014), contours are shown at 250 m intervals. Bathymetric data are from Jakobsson *et al.* (2012), contours are shown at 100 m intervals to -1000 m, and 500 m intervals below this. Camel plots generated using Matlab after Balco (2011). Erratic ^{10}Be exposure ages are shown in blue. Bedrock ^{10}Be exposure ages are shown in magenta. The timing of deglaciation at each site is shown by the dashed line, errors are shown by the grey shaded area. The inset graph shows the latitudinal trend in the deglaciation of high discharge glacier systems. The linear regression excludes samples from Tugtilik (hollow circles). Samples are colour grouped by sampling site and show individual internal uncertainties.

Table 1: Sample details and ^{10}Be age determinations. Exposure ages were calculated using the Arctic production rate (Young *et al.*, 2013) and Lal/Stone time-independent scaling (Lal, 1991; Stone, 2000).

Sample ID	AMS ID	Lat.	Long.	Elevation (m asl)	Sample type	Lithology	Thickness (cm)	Density (g cm^{-3})*	Shielding Correction†	^{10}Be (atoms g^{-1})	^{10}Be uncertainty (atoms g^{-1})	Exposure Age (yr.) zero erosion	Internal Uncertainty (yr.)	External Uncertainty (yr.)
Tugtilik														
MF1101	b9337	66.347	-34.98	152	Erratic	Gneiss	4.7	2.67	0.9902	52646	2007	**10953**	419	592
MF1102	b9338	66.347	-34.979	154	Erratic	Gneiss	4.1	2.66	0.9902	44991	1823	**9291**	377	518
MF1103	b9341	66.347	-34.98	152	Bedrock	Gneiss	4.5	2.68	0.9902	47080	1868	**9778**	389	539
Ikertivaq														
IK1101	b9331	65.467	-39.228	67	Erratic	Gneiss	4.75	2.71	0.9997	44235	1900	**9925**	427	572
IK1102	b9332	65.467	-39.228	67	Bedrock	Gneiss	5.4	2.79	0.9997	50437	3106	**11394**	704	828
Køge Bugt														
KB1103	b9334	64.97	-40.076	50	Erratic	Gneiss	4.15	2.65	0.9999	49538	1959	**11182**	443	616
KB1105	b9335	64.97	-40.076	50	Bedrock	Pale Gneiss	4.4	2.68	0.9999	40849	1791	**9238**	406	538
KB1106	b9336	64.97	-40.076	51	Bedrock	Gneiss	4.55	2.68	0.9999	46469	1899	**10514**	431	589
Gerners Island														
GY1107	b9328	64.361	-40.323	113	Erratic	Gneiss	3.8	2.73	0.9991	46783	2264	**9838**	477	608
GY1108	b9329	64.361	-40.321	128	Erratic	Pink Gneiss	3.95	2.73	0.9964	48375	2106	**10052**	439	583
GY1109	b9330	64.361	-40.321	128	Bedrock	Gneiss	3.9	2.62	0.9989	53662	1983	**11109**	412	592

*Density measured from subsamples; mean density of all samples from Køge Bugt used for KB1105 and KB1106.

†Topographic shielding corrections were calculated using the CRONUS-Earth online calculator: http://hess.ess.washington.edu/math/general/skyline_input.php.